Improvement of small to large grain A15 ratio in Nb_3Sn PIT wires by inverted multistage heat treatments

IOP Conf. Series: Materials Science and Engineering **279** (2017) 012019 doi:10.1088/1757-899X/279/1/012019

Improvement of small to large grain A15 ratio in Nb_3Sn PIT wires by inverted multistage heat treatments

Christopher Segal, Chiara Tarantini, Peter J Lee and David C Larbalestier

Applied Superconductivity Center, NHMFL, Florida State University, Tallahassee, FL 32310, USA

E-mail: segal@asc.magnet.fsu.edu

Abstract. The next generation of superconducting accelerator magnets for the Large Hadron Collider at CERN will require large amounts of Nb_3Sn superconducting wires and the Powder-In-Tube (PIT) process, which utilizes a $NbSn_2$-rich powder core within tubes of Nb(7.5wt%Ta) contained in a stabilizing Cu matrix, is a potential candidate. However, the critical current density, J_c, is limited by the formation of a large grain (LG) A15 layer which does not contribute to transport current, but occupies 25-30% of the total A15 area. Thus it is important to understand how this layer forms, and if it can be minimized in favor of the beneficial small grain (SG) A15 morphology which carries the supercurrent. The ratio of SG/LG A15 is our metric here, where an increase signals improvement in the wires A15 morphology distribution. We have made a critical new observation that the initiation of the LG A15 formation can be controlled at a wide range of temperatures relative to the formation of the small grain (SG) A15. The LG A15 can be uniquely identified as a decomposition product of the $Nb_6Sn_5(Cu_x)$, surrounded by a layer of rejected Cu, thus the LG A15 is not only of low pin density, but is not continuous grain to grain. We have found that in single stage reactions limited to 630 °C - 690 °C, the maximum SG A15 layer thickness prior to LG A15 formation is very sensitive to temperature, with a maximum around 670 °C. This result led to the design of four novel heat treatments which all included a short, high temperature stage early in the reaction, followed by a slow cooling to a more typical reaction temperature of 630 °C. We found that this heat treatment (HT) modification increased the SG A15 layer thickness while simultaneously suppressing LG A15 morphology, with no additional consumption of the diffusion barrier. In the best heat treatment the SG/LG A15 ratio improved by 30%. Unfortunately, J_c values suffered slightly, however further exploration of this high temperature reaction region is required to understand the limits to A15 formation in Nb_3Sn PIT conductors.

1. Introduction

The Powder-In-Tube (PIT) manufacturing process has been used to produce multifilament Nb_3Sn wires for over 30 years [1]. Starting with the earliest variants at ECN, followed by Shape Metal Innovations (SMI), and today Bruker EAS, three morphologies of Nb_3Sn A15 grains are always formed during the reaction; a small grain (SG), a large grain (LG), and fully disconnected core grains (figure 1). The small grain ($\sim$ 150 nm) region forms from Sn contained in Nb_6Sn_5 diffusing into the Nb(Ta) tube, while the the large (>1 μm) and core grains were observed to have formed from decomposition of the $Nb_6Sn_5(Cu_x)$ layer which precedes the A15 reaction [2, 3]. It should be noted that although LG A15 does form in the internal Sn method [4], it is typically $<$ 5 vol% of the A15 area. Given this state of the art conductor, the recommendations to improve the

PIT method are to consume more diffusion barrier without loss of RRR [5] and to suppress the formation of LG A15 as it does not contribute to transport current but occupies 25-30% of the total A15 area [6, 7]. A metric we will use here to determine if the microstructure has improved is the SG/LG ratio of the A15 morphologies, where a higher number is better. In order to suppress the LG A15, we first needed to develop a better understanding of its formation, as well as the formation of the A15 precursor phases Nausite [8], $NbSn_2$ and Nb_6Sn_5 by microstructural and chemical analysis.

2. Experimental Details

The wire studied is 0.78 mm in diameter from billet B31284 manufactured by Bruker EAS, and contains 192 filaments with diameter of $\sim$39 μm set in a Cu stabilizer (Figure 1). Each filament consists of a thick Nb-7.5wt%Ta tube clad in Cu and filled with a Sn-rich powder mixture typically containing $NbSn_2$, Sn and Cu [9]. A thin Cu sleeve separates the powder from the inner tube wall. Such a monofilament is drawn, cut and stacked multiple times until the desired architecture is achieved; here a 192 filament wire.

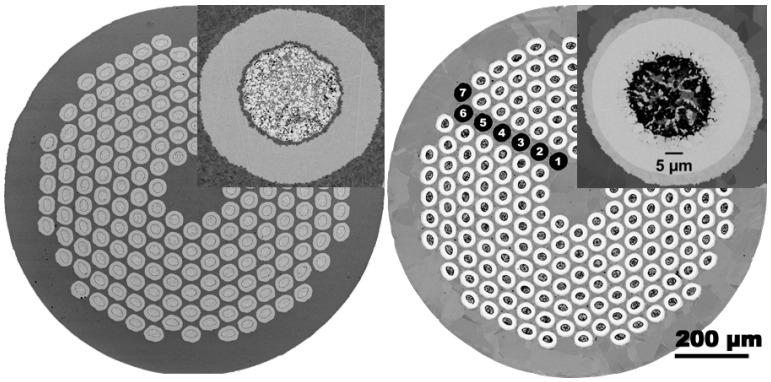

Figure 1: FESEM-BSE images of polished, transverse cross-sections of an unreacted (left) and reacted (right) Bruker PIT wire 1 mm in diameter with 192 superconducting filaments within a matrix of stabilizing Cu. Inset image is of a typical round filament

To study the phase and morphology evolution in these Nb_3Sn wires, a series of quench experiments were performed in which short samples of wire were removed from the reaction furnace at key times to better understand the microstructural evolution. Wires were cut into 10 cm lengths, the ends were crimped shut, and sealed in an evacuated quartz tube in which a small amount of argon ($\sim$ 300 torr) was introduced to promote heat transfer. These samples were then stacked in the furnace, and individually pulled out into an ice bath to "freeze" the microstructure. The wires were then mounted in a conductive puck and polished for imaging in a Scanning Electron Micropscope (SEM).

Digital Imaging was performed using a Zeiss 1540 Crossbeam Field Emission Scanning Electron Microscope (FESEM). The back scattered electron (BSE) intensity in the FESEM is sensitive to atomic number (Z) and phases with a higher effective Z are brighter in the BSE image, as seen in Figure 1. These data combined with knowledge of the phase diagrams for Cu-Sn [10] and Nb-Sn [11, 12] allow quick identification of the Cu, Nb-7.5wt%Ta, and the $Nb(Ta)_3Sn$ phases. We can also measure the area fractions of each phase with the widely used open-source software package, FIJI [13] (based on Image J [14]), allowing us to make high precision comparisons between samples.

Critical current (I_c) measurements were made in a 15 T solenoid using four-point measurements on 4.5 cm long straight samples with voltage taps in the center 1 cm apart. A voltage criterion of 1 μV/cm was used to determine the superconducting transition. To compare wires with different architectures we can normalize the critical current over the non-Cu area to determine a critical current density (J_c). Furthermore, we can measure the quality of the

superconducting A15 phase by normalizing I_c over only the current carrying small-grain A15 layer to determine a layer J_c ($J_{c-layer}$).

3. Results

3.1. Phase Evolution under 630 ˚C, prior to A15 formation

The phase diagrams for Cu-Sn and Nb-Sn allow us to anticipate the phases that will be produced as the reaction proceeds. For the following discussion the values of interest are similar, and either phase diagram can be used. First we consider the starting wire in an unreacted state as seen in the left side of Figure 1. As the heat treatment begins, Sn is rapidly absorbed into the α-Cu sleeve and transforms to the most Sn rich Cu-Sn compound, η (Figure 2). The η phase metlts at 408 °C, and as the reaction proceeds, the η begins converting into ϵ which remains as the dominant Cu-Sn phase until sufficiently depleted of Sn towards the end of the reaction. In addition to the described Cu-Sn phase formation, there is a ternary Sn-Nb-Cu phase called Nausite [8] that forms as early as 200 °C [15]. The structure and composition of Nausite has recently been reported to be $(Nb_{0.75}Cu_{0.25})Sn_2$ [16].

Above 408 °C, both the Nausite and ϵ phase grow in thickness until about 560 °C, at which point the Nausite decomposes into $NbSn_2$, rejecting its Cu. The $NbSn_2$ is rather short lived, and at 630 °C transforms to Nb_6Sn_5, containing up to 5at%Cu, in less than an hour (Figure 2).

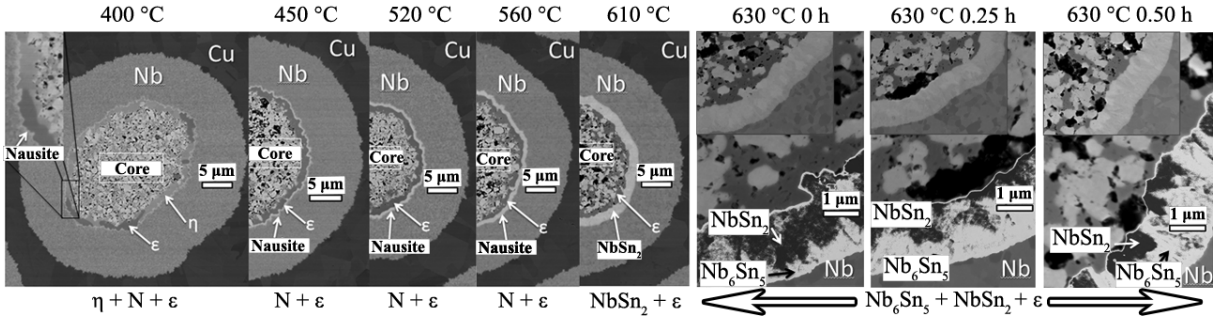

Figure 2: FESEM-BSE images of polished, transverse cross-sections showing phase evolution up to 610 °C. In the 630 °C panels the Nb-Sn phases have bee contrast enhanced at the DB interface to better distinguish phases, original images are inset. A thin light ring of Nausite (N) has formed on heating to 400 °C and continues to grow until about 610 °C when it decomposes into $NbSn_2$. The Cu-Sn phase has a transformation from η to ϵ + liquid at 408 °C which remains as the dominant Cu-Sn phase until sufficiently depleted of Sn towards the end of the reaction.

3.2. A15 growth at 630 ˚C

At 630 °C, the dominant phase kinetics are for the $Nb_6Sn_5(Cu_x)$ to feed Sn to the Nb-Ta tube and form SG A15. Already at only five hours, we see a thin layer of SG A15 form between the DB and the $Nb_6Sn_5(Cu_x)$ layer at the edge of the core (Figure 3). At 10 h the SG A15 layer thickness more than doubled to 0.85 μm. By 12 h, the $Nb_6Sn_5(Cu_x)$ begins to decompose into large grains of A15 at the interface with the SG A15 layer, ejecting Cu into mesoscopic precipitates at the large grain boundaries. The appearance of the Cu is not surprising as it is well known that Nb_3Sn does not dissolve any Cu [17]. By 30 h much LG A15 has formed with the surrounding Cu ejected during the transformation. Meanwhile, SG A15 continues to grow. At 58 h there is a SG A15 layer ~3.4 μm thick, the LG A15 layer growing appreciably, with a now fully continuous Cu-Sn phase (ϵ) separating the A15 phases from the remaining $Nb_6Sn_5(Cu_x)$. The $Nb_6Sn_5(Cu_x)$ is fully consumed around 100 h. However, there is significant Sn left stranded in the core that could form more A15 by continued reaction. Once the reaction is completed around 240 h, 58.1% of the filament area is A15. This 58.1% volume of A15 is composed of

3 morphologies; 40.7% SG A15 (5-5.5 μm thick), 14.4% LG A15 (2.5 μm thick), and 3.0% of porous, disconnected core grains of A15. Important to note is that only the SG A15 carries the transport current [7], meaning that 30% of the A15 is useless in the current conductor design. From the critical viewpoint of making PIT more attractive as a high J_c conductor, we need to fully understand why the LG A15 forms, and if it can be suppressed in favor of the desirable SG A15.

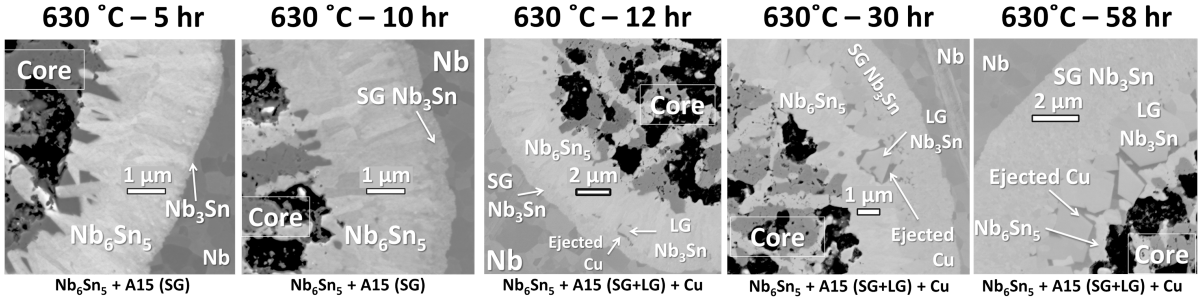

Figure 3: FESEM-BSE images of polished, transverse cross-sections showing A15 phase growth at 630 °C. The SG A15 layer steadily grows, with LG A15 nucleating around 12 h. By 58 h most of the Nb_6Sn_5 is gone, and we have continuous layers of SG A15, LG A15, and Cu phases which separates the Nb_6Sn_5 from being in direct contact with the SG A15 layer.

3.3. Heat treatment effects on A15 morphology early in the reaction

The temperature of the A15 reaction has a substantial influence on the formation of LG A15 early in the reaction [3]. At 675 °C reference [3] found a much thicker layer of SG A15, than what was described here at 630 °C when only one large A15 grain has formed (Figure 4). This is a surprising result because at 630 °C the thickness of the SG A15 layer is less than a micron when LG A15 starts nucleate, but at 675 °C the SG A15 layer has doubled in thickness to about 2 μm.

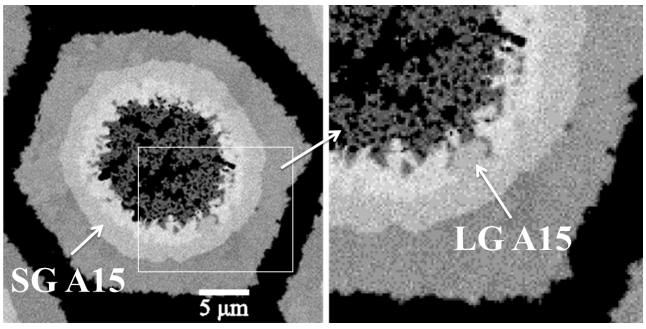

Figure 4: One filament from a wire produced by SMI heat treated at 675 °C for 4 h. There is already a thick layer of SG A15, and one large A15 grain has formed in the Nb_6Sn_5 layer with Cu ejected around it [3].

Previously, we have analyzed the SG/LG ratio of 10 PIT wires differing by either HT or billet design, and found that the total A15 volume fraction varies only slightly from 55-58% in fully reacted samples [5], with the SG/LG ratio varying from 2.4-3.0. However, the vintage SMI PIT sample in Figure 4 shows that the ratio of SG/LG A15 does vary substantially early in the reaction as a function of HT temperature, when LG A15 is just forming. Consequently we performed a study on the phase morphology variation as a function of temperature early in the HT, performing single stage HT's which all ramped up at 100 °C/h to a dwell temperature of either 630, 650, 670, or 690 °C for between 50-250 h. For this experiment we obtained about 50 m of conductor at 0.78 mm wire diameter through the LARP collaboration (details in section 5).

The focus of these heat treatments was to observe the early stages of the reaction by quenching samples to compare the rates of SG and LG A15 growth as a function of dwell temperature.

In all cases, the SG A15 formed first, and the LG A15 formed later in the A15 reaction, and more rapidly at higher temperatures. From our quench experiment at 630 °C we found that the LG A15 started forming around 12 h, with a SG A15 layer thickness of 0.85 μm. At 650 °C the SG A15 layer was 1.5 μm thick and the LG A15 first precipitates out after 8.3 h. At 670 °C the LG A15 begins forming after only 5 h, and the SG A15 layer formed is 2 μm thick. At 690 °C the SG layer thickness is only 1.6 μm with LG A15 forming in less than two hours (Figure 5). If we take this data and create an isothermal transformation diagram for A15 morphology, we see a clear boundary for LG formation (Figure 6). This isothermal transformation diagram incited us to develop a new type of multi-temperature A15 reaction in which we start with a brief high temperature excursion to grow a thick SG A15 layer, then drop the temperature to minimize LG A15 formation.

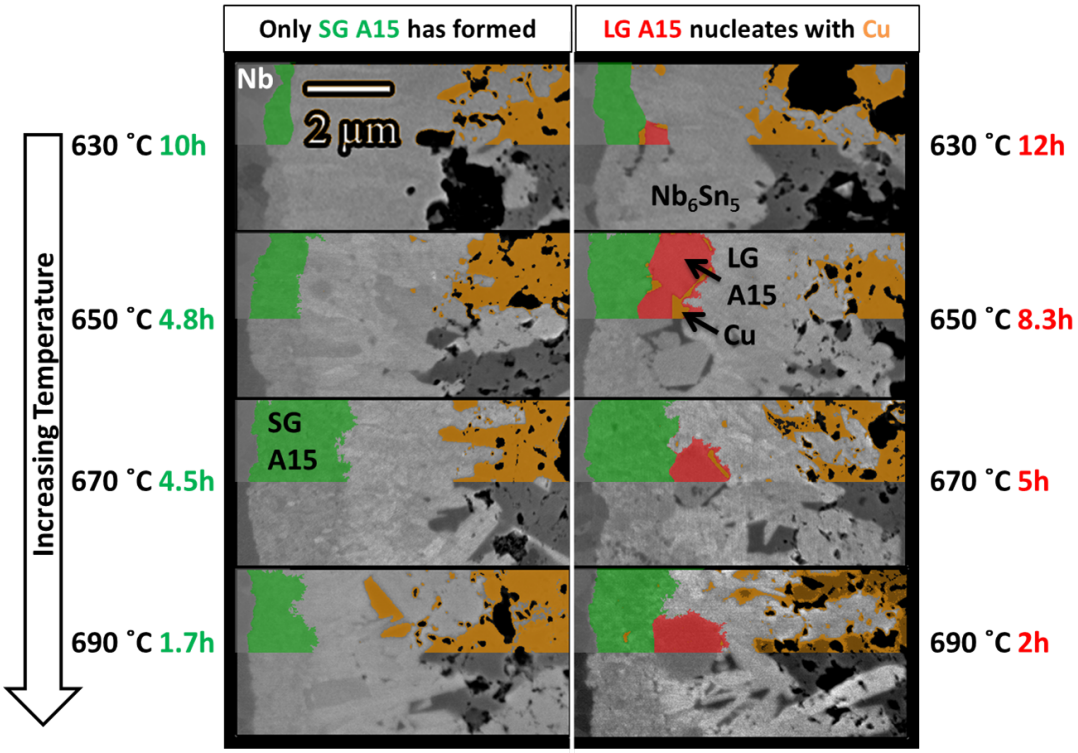

Figure 5: Micrographs of the LG A15 nucleation. From top to bottom the reaction temperature increases from 630 to 650, 670, and 690 °C. The left column shows images of SG A15 before LG A15 formation (<1% of the filament cross section). The right column is after LG A15 has formed. Half of each panel is colored to distinguish between phases and the two A15 morphologies. Considering a panel from the right column, from left to right, we see: Nb-Ta DB, SG A15, LG A15 (with Cu precipitates), Nb_6Sn_5, and core remnants containing Cu and voids (black)

3.4. Inverted multistage heat treatments benefit the small grain/large grain A15 ratio

In an attempt to avoid or delay the LG nucleation as suggested by the previous experiment in section 3.3, we designed four "inverted multistage" HT's. A typical HT from the manufacturer may contain multiple stages, but always increasing in temperature, a standard BEAS HT for example is 620 °C 100 h + 640 °C 12 h. Here we invert this by first going to a high temperature, and then cooling to the final A15 reaction temperature. The components of this new HT design can be summarized as:

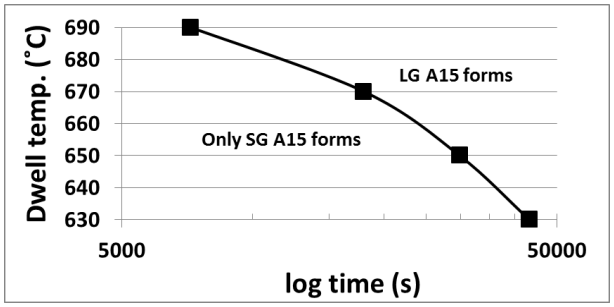

Figure 6: Isothermal transformation curve showing how temperature and time effect the onset of large grain A15 formation in single dwell HT's. The line is generated from the right column of Figure 5 and is an approximate boundary for when LG A15 will form.

- Ramp-up to the highest reaction temperature (HRT) (670 °C - 690 °C).
- Short dwell at HRT (including no dwell in some cases) (0 - 3.5 h)
- Ramp-down to the low-temperature reaction (LTR) dwell. (5 - 20 °C/h)
- Long LTR dwell (190 - 220 h)

For the purpose of this experiment we wanted to optimize the HRT, HRT dwell time, and ramp-down to the LTR dwell such that large grains of A15 have not yet formed, and we have maximized the SG A15 layer thickness.

3.4.1. Microstructures early in the the inverse multistage heat treatment Early in the inverse multistage HT's, The SG/LG ratio is quite variable since LG A15 can be substantially delayed while growing SG A15. The results are summarized in Table 1. Our first HT (A) nucleated large grains about 13 h into the LTR dwell at 630 °C with a SG layer thickness of 2.2 μm, a 10 % improvement over the best single step SG A15 layer thickness observed at 670 °C with no LG A15 (Figure 7). HT C was the best at delaying LG A15 while producing the most SG A15 early in the reaction as seen in Figure 7.

Table 1: Early microstructure of the four wires heat treated using inverse multistage heat treatments, and two single stage HT wires included for reference. The SG A15 layer thickness is measured when there is 1vol% LG A15.

HT (°C)	HRT	SG layer thickness (μm)
630	630	0.85
670	670	2.0
Inverse Multistage HT A	690	2.2
Inverse Multistage HT B	690	2.7
Inverse Multistage HT C	690	3.0
Inverse Multistage HT D	670	2.2

3.4.2. Phase and microstructure after full reaction The results of the four inverse multistage HT's after a full reaction are compiled in Table 2. The most notable were the SG A15 improving from 40 to 44% while the LG A15 decreased from 13.3 to ~11.8%, the core A15 being halved. This led to an improved SG/LG A15 ratio in all HT's, the highest being 3.9 compared to 2.8 in a standard HT. Heat treatments B and C had very similar SG/LG A15 ratios, however HT C had an additional 1.5% of total A15 (Figure 8).

3.4.3. Electrical properties after full reaction To compare I_c values of the inverse multistage HT's to the standard HT of 620/100 + 640/90. I_c values of HT's B, C, and D varied by less than 1%, from 489-493 A; about 2% less than the standard wire (Table 2). However, I_c is

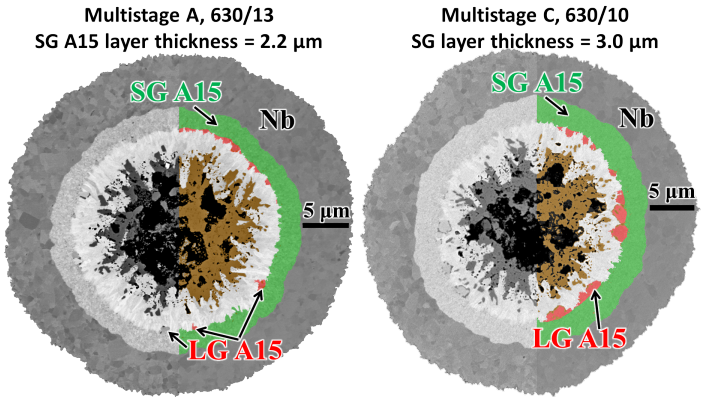

Figure 7: HT A and C are compared as the LG A15 is forming. Filaments are half colored to distinguish between phases. The SG layer thickness of HT C after 10 h in the LTR dwell is 3 μm.

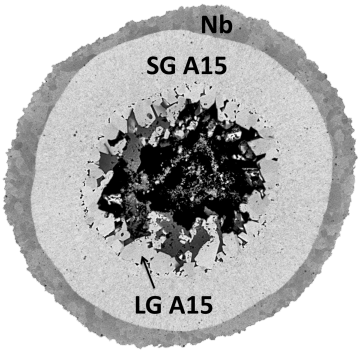

Figure 8: A filament from HT C reacted at a LTR dwell at 630 °C for 210 h. The large A15 grains were reduced, and are very loosely connected to the SG A15 layer.

strongly dependent on the amount of SG A15, and its grain size. We can better understand the differences between HT's by normalizing critical current to the SG A15 layer for each sample since only that layer carries current. A wire reacted with a standard HT has a $J_{c-layer}$(12 T, 4.2 K) of 5564 A/mm^2, while the best HT (C) had a $J_{c-layer}$(12 T, 4.2 K) of only 4926 A/mm^2, a substantial drop. Heat treatments C and D had very similar layer J_c(12 T, 4.2 K) which is 10% lower than a wire with standard HT. By staying below 670 °C we were able to recover some of the layer J_c (12 T, 4.2 K), increasing from about 4950 A/mm^2 in HT B & C to 5150 A/mm^2 in HT D, however, less A15 is produced overall.

Table 2: Fully reacted microstructure and J_c(12 T, 4.2 K) of wires heat treated using inverse multistage heat treatments, and the standard HT BEAS wire included for reference.

			Electrical Properties			Phase or morphology volume %						
HT (°C)	HRT (°C)	Time in LTR dwell (h)	I_c(A)	J_c non-Cu	J_c layer	DB	A15 total (S+L+C)	Remnant core	A15 SG	A15 LG	A15 core	SG/LG ratio
620+640	-	100+90	501	2237	5564	23.4%	56.0%	20.6%	40.2%	13.3%	2.5%	3.0
Inverse Multistage HT A	690	220	-	-	-	25.4%	56.3%	18.4%	43.5%	12.0%	0.8%	3.6
Inverse Multistage HT B	690	190	489	2183	4958	24.4%	56.0%	19.4%	44.0%	11.2%	0.8%	3.9
Inverse Multistage HT C	690	210	491	2192	4926	24.0%	57.3%	18.7%	44.5%	11.6%	1.2%	3.8
Inverse Multistage HT D	670	210	493	2201	5137	24.5%	56.6%	18.9%	42.8%	12.4%	1.3%	3.5

4. Discussion

For all heat treatments the SG A15 formed before LG A15. We found that the SG/LG A15 ratio can be increased, but only by going about 60 °C above the standard HT temperatures. The final A15 volume of all inverse multistage HT wires were similar, ~43-44.5%, but produced different $J_{c-layer}$ values, attributed to both the HRT of the HT as well as the temperature at which A15 is formed. Heat treatments with HRT of 690 °C showed about a 12% decrease in 12 T $J_{c-layer}$, while an HRT of 670 °C showed only an 8% decrease over the standard HT. We believe this difference is due to the average grain size being higher for the SG A15 which forms $>$ 670 °C, and was the motivation for HT D having a maximum of 670 °C, in an effort to keep the grain size small. This was successful as the $J_{c-layer}$ improved from HT C, but not as high as the standard BEAS HT. While all HT's improved the SG/LG A15 ratio, the lowest was HT

D which had an HRT of only 670 °C. Our observation is that higher temperatures (>670 °C) tend to either 'push' the core material to the tube wall, or agglomerates voids in the center of each filament. In either case, the result is that nearly all Sn in the core has a clearly connected diffusive path to react with the Nb(Ta) tube. At lower temperatures there tends to be many small voids in the core, leading to Sn being trapped and eventually transforming into A15 as seen in Figure 1. With the SG/LG ratio now improved, we need to find an optimized HRT which still allows the most Sn to react with the tube wall, but without causing the small grains of A15 to grow too large.

5. Conclusion

One possible method to improve Nb_3Sn PIT wires is to suppress LG A15 formation in favor of SG A15. There is a complex succession of phases which form and decompose until finally the A15 reaction temperature is reached (> 630 °C), where the dominant kinetics are for $Nb_6Sn_5(Cu_x)$ to feed Sn into the NbTa tube to form SG A15. A higher reaction temperature allows greater delivery of Sn to the Nb-Ta tube for more SG A15, but has yet to prevent the LG A15 from forming, which seems to be the exhaustion point of the original $NbSn_2$ core. A series of isothermal HT studies encouraged us to design new inverted multistage HT's with a short high temperature spike in the beginning to rapidly grow the SG A15 before LG A15 forms. These HT's achieved a 50% increase to SG A15 layer before LG A15 nucleated out of the $Nb_6Sn_5(Cu_x)$ in the early hours of the reaction. After a full reaction, the SG A15 layer increased by 10%, while the LG A15 decreased 10-15%, and the core A15 was halved, improving the SG/LG ratio from 3.0 to 3.9. Unfortunately, J_c(12 T,4.2 K) suffered, dropping by as much as 10%. We believe that large variations in the SG/LG A15 ratio early in the A15 reaction window can be improved by further optimization of inverted multistage HT's. While the J_c(12 T) is sensitive to grain size, typically restricting reactions <670 °C, the higher temperature HT's may be more favorable for 15-16 T applications once fully optimized.

Acknowledgments

Acknowledgments All experiments were carried out on Billet 31284, supplied to us by LBNL through the US LHC Accelerator Research Program (LARP), which is a BNL, FNAL, LBNL, and SLAC collaboration with CERN for the High Luminosity LHC program. The wire was received at 0.79 mm diameter in the unreacted condition. This work was supported by the US Department of Energy (DOE) Office of High Energy Physics under award DE-SC0012083, by CERN, and by the National High Magnetic Field Laboratory (which is supported by the National Science Foundation under NSF/DMR-1157490), the State of Florida, and CERN under grants KE1920/TE and RF02226

References

[1] Beijnen C van and Elen J. "Multifilament Nb_3Sn superconductors produced by the E.C.N. technique". Version 2. In: *IEEE Transactions on Magnetics* 15.1 (1979), pp. 87–90.

[2] Veringa H, Hoogendam P and Wees A. "Growth kinetics and characterization of superconducting properties of multifilament materials made by the ECN powder method". Version 2. In: *IEEE Transactions on Magnetics* 19.3 (May 1983), pp. 773–776.

[3] Hawes CD. "Investigations of the Inhomogeneity of a Powder-In-Tube Nb_3Sn Conductor". PhD thesis. University of Wisconsin - Madison, 2000.

[4] Michiel MD and Scheuerlein C. "Phase transformations during the reaction heat treatment of powder-in-tube Nb_3Sn superconductors". Version 2. In: *Superconductor Science and Technology* 20.10 (Oct. 1, 2007), p. L55.

[5] Segal C et al. "Evaluation of critical current density and residual resistance ratio limits in powder in tube Nb_3Sn conductors". Version 2. In: *Superconductor Science and Technology* 29.8 (2016), p. 085003.

[6] Godeke A et al. "State of the art powder-in-tube niobium–tin superconductors". Version 2. In: *Cryogenics* 48.7 (July 2008), pp. 308–316.

[7] Tarantini C et al. "Composition and connectivity variability of the A15 phase in PIT Nb_3Sn wires". Version 2. In: *Superconductor Science and Technology* 28.9 (Sept. 1, 2015), p. 095001.

[8] Naus M, Lee P and Larbalestier D. "The influence of the starting Cu-Sn phase on the superconducting properties of subsequently reacted internal-Sn Nb_3Sn conductors". Version 2. In: *IEEE Transactions on Applied Superconductivity* 11.1 (Mar. 2001), pp. 3569–3572.

[9] Godeke A. "Performance Boundaries in Nb_3Sn Superconductors". PhD thesis. University of Twente, 2005.

[10] Fürtauer S et al. "The Cu–Sn phase diagram, Part I: New experimental results". Version 2. In: *Intermetallics* 34 (Mar. 2013), pp. 142–147.

[11] Charlesworth JP, Macphail I and Madsen PE. "Experimental work on the niobium-tin constitution diagram and related studies". Version 2. In: *Journal of Materials Science* 5.7 (July 1970), pp. 580–603.

[12] Toffolon C et al. "Reassessment of the Nb-Sn system". Version 2. In: *Journal of Phase Equilibria* 23.2 (Mar. 1, 2002), pp. 134–139.

[13] Schindelin J et al. "Fiji: an open-source platform for biological-image analysis". Version 2. In: *Nature Methods* 9.7 (July 2012), pp. 676–682.

[14] Schneider CA, Rasband WS and Eliceiri KW. "NIH Image to ImageJ: 25 years of Image Analysis". In: *Nature methods* 9.7 (July 2012), pp. 671–675.

[15] Pong I, Oberli LR and Bottura L. "Cu diffusion in Nb_3Sn internal tin superconductors during heat treatment". Version 2. In: *Superconductor Science and Technology* 26.10 (Oct. 1, 2013), p. 105002.

[16] Martin S et al. "The crystal structure of $(Nb_{0.75}Cu_{0.25})Sn_2$ in the Cu-Nb-Sn system". Version 2. In: *Intermetallics* 80 (2017), pp. 16–21.

[17] Yamashina T and Kajihara M. "Quantitative Explanation for Uphill Diffusion of Sn during Reactive Diffusion between Cu-Sn Alloys and Nb". Version 2. In: *MATERIALS TRANSACTIONS* 47.3 (2006), pp. 829–837.